Band-stop filters based on a coupled circular ring metal–insulator–metal resonator containing nonlinear material

2012 J. Opt. 14 055001

(http://iopscience.iop.org/2040-8986/14/5/055001)

J. Opt. **14** (2012) 055001 (6pp) doi:10.1088/2040-8978/14/5/055001

Band-stop filters based on a coupled circular ring metal–insulator–metal resonator containing nonlinear material

Gaige Zheng[1], Wei Su[2], Yunyun Chen[1], Chengyi Zhang[1], Min Lai[1] and Yuzhu Liu[3]

[1] School of Physics and Optoelectronic Engineering, Nanjing University of Information Science and Technology, Nanjing 210044, Jiangsu, People's Republic of China
[2] School of Science, Nanjing University of Science and Technology, Nanjing 210094, Jiangsu, People's Republic of China
[3] Paul Scherrer Institute, WSLA-004, Villigen CH5232, Switzerland

E-mail: jsnanophotonics@yahoo.com

Received 29 September 2011, accepted for publication 1 March 2012
Published 27 March 2012
Online at stacks.iop.org/JOpt/14/055001

Abstract
An all-optical plasmonic filter based on a metal–insulator–metal (MIM) waveguide coupled with a circular ring resonator containing a Kerr nonlinear medium is proposed and numerically investigated. The optical filtering effect is verified by the finite difference time-domain (FDTD) method and the simulation results reveal that the increase in the refractive index induced by enhancing the incident intensity can cause a red-shift for the resonance wavelengths. Thus the resonant wavelengths can be tuned without changing the outer size of the structure. The proposed band-stop plasmonic filter is of a compact size that has potential application for integrated optics in which we have limitations on the outer dimensions and it is not possible to enlarge the dimension of the ring resonator to reach longer resonant wavelengths.

Keywords: surface plasmons, plasmonic filter, optical resonators, metal–insulator–metal

(Some figures may appear in colour only in the online journal)

1. Introduction

Surface plasmon-based devices have attracted tremendous interest from researchers in recent years because of their outstanding performance in guiding and manipulating light at deep sub-wavelength scales resulting from the strong localization of surface plasmon polaritons (SPPs) [1–3]. Plasmonic waveguides are important structures in plasmonic devices based on SPPs propagating at metal–dielectric interfaces [4–10]. There are two important kinds of plasmonic waveguide, i.e. insulator–metal–insulator (IMI) and metal–insulator–metal (MIM) waveguides. IMI waveguides have a lower loss but poor capability to confine light on a sub-wavelength scale, while MIM waveguides are becoming increasingly popular because they can not only support modes with deep sub-wavelength scales and high group velocity over a very wide range of frequencies [7, 9], but can also provide long-range propagation and allow the manipulation and transmission of light at the nano-scale. Various passive MIM waveguide components have been demonstrated by numerical simulations and experiments, such as Mach–Zehnder interferometers [4, 5], biosensors [6], Bragg reflectors [7–10], ring resonators [11], optical buffers [12] and so on. To overcome the complexity of fabrication of Bragg reflectors operated as good band-stop filters, plasmonic waveguide filters have been proposed and demonstrated, such as tooth-shaped waveguide filters [13–15], coupler-type filters [16], channel drop filters with disk resonators [17], rectangular geometry resonators [18, 19], and ring resonators [11, 20, 21]. At the same time, optical nonlinear effects have been shown to be an

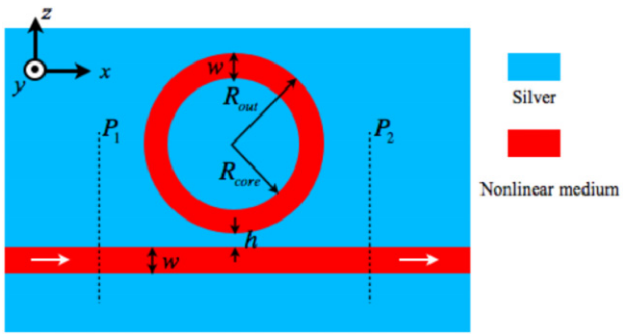

Figure 1. Schematic structure of a plasmonic filter structure where a circular ring resonator filled with nonlinear material is coupled to a bus waveguide. w, h, R_{core} and R_{out} are the width of the MIM waveguide, the gap distance between the input/ output MIM waveguides and the circular ring resonator, the radius of core and the outer radius of the ring resonator, respectively.

attractive approach for active control of the optical signal in plasmonic devices because of their operation in an all-optical fashion with an ultra-fast response time [22–28].

In this paper, we make an analytical and numerical study of the transmission response of a nano-scale system consisting of a MIM waveguide and a circular ring resonator filled with nonlinear medium. By incorporating a circular ring resonator filled with nonlinear material into the MIM waveguide, the transmission response of the combined structure can be modified; this will be verified by the finite difference time-domain (FDTD) method. The transmission spectrum of this system possesses obvious and sharp valleys and the resonance wavelength of the cavity exhibits a red-shift with increasing incident intensity. As a consequence, the resonant wavelengths can be tuned without changing the outer size of the structure. Such features may be potentially applied to constructing SPP-based all-optical filters in the case of integrated circuits.

2. Structures and simulation method

Figure 1 shows the structure of a simple band-stop plasmonic filter which consists of a MIM waveguide laterally coupled to a circular ring resonator containing a nonlinear medium. The filter parameters w, h, R_{core} and R_{out} are the width of the MIM waveguide, the gap distance between the input/output MIM waveguide and the circular ring resonator, the radius of the core and the outer radius of the ring resonator, respectively. We set $w = 50$ nm, which is much smaller than the operating spectrum. Two power monitors are set at points P_1 and P_2 to detect the input power A_1 (without the circular ring resonator) and the transmitted power A_2 (with the circular ring resonator). So, the power transmittance is $T = A_2/A_1$ [11].

The metal is chosen as silver in this paper and the frequency-dependent relative permittivity can be characterized by the Drude model [29]:

$$\varepsilon_{\text{m}}(\omega) = \varepsilon_\infty - \frac{\omega_{\text{p}}^2}{\omega^2 + \text{j}\gamma_{\text{p}}\omega}. \tag{1}$$

Here ε_∞ is the dielectric constant at infinite angular frequency and ω_{p} and γ_{p} are the plasma and collision angular frequencies, respectively. All the parameters of the Drude model can be found in [30, 31]. The ring resonator is filled with a Kerr medium whose dielectric constant depends on the intensity of incident light [24, 25]:

$$\varepsilon_{\text{d}} = \varepsilon_{\text{l}} + \chi^{(3)}|E|^2 \tag{2}$$

where ε_{l} is the linear dielectric constant, set as 2.25, the third-order nonlinear susceptibility $\chi^{(3)}$ is chosen as a typical value for nonlinear optical materials such as InGaAsP, that is $\chi^{(3)} = 4 \times 10^{-18}$ m^2 V^{-2} [30].

The FDTD method is used to study the transmission properties of this cavity structure, with perfectly matched layer (PML) absorbing boundary conditions in the x and z directions of the simulation domain. In the following FDTD simulations the grid size in the x and z directions are chosen to be $\Delta x = \Delta z = 2$ nm and $\Delta t = \Delta x/2c$, which are sufficient for numerical convergence; here c is the velocity of light in a vacuum. The auxiliary differential equation (ADE) method is used to simulate dispersive media. To simulate the performance of our proposed devices, we have solved Maxwell's equations and imported the nonlinear polarization vector to the Maxwell equation of our FDTD program:

$$\nabla \times \mathbf{E} = -\mu\frac{\partial}{\partial t}\mathbf{H} \qquad \nabla \times \mathbf{H} = \frac{\partial}{\partial t}\mathbf{D}$$
$$\mathbf{D} = \varepsilon_0\varepsilon_\infty\mathbf{E} + \mathbf{P}_{\text{L}} + \mathbf{P}_{\text{NL}} \tag{3}$$

where ε_0 is the free space permittivity and $\mathbf{P}_{\text{L}}$ and $\mathbf{P}_{\text{NL}}$ are the linear and nonlinear polarization vectors related to the Drude model and Kerr nonlinearity, respectively:

$$\frac{\partial^2\mathbf{P}_{\text{L}}}{\partial t^2} + \gamma_{\text{p}}\frac{\partial\mathbf{P}_{\text{L}}}{\partial t} = \varepsilon_0\omega_{\text{p}}^2\mathbf{E} \qquad \mathbf{P}_{\text{NL}} = \varepsilon_0\chi^{(3)}\mathbf{E}^3. \tag{4}$$

To excite the SPPs, a TM polarized plane wave whose magnetic field is parallel to the y axis is launched to the plasmonic filter structure of figure 1. The transmission of all the proposed devices is normalized to the transmission of a straight MIM waveguide with the same parameter.

3. Band-stop MIM filter with a circular ring resonator containing a linear medium

The manipulation of coupling between MIM waveguides and micro-resonators is shaping up as an important area of research and development. The transmission of an all-pass ring resonator has been given in [32]; it was assumed that there is no loss in the coupling region, which is not true for plasmonic devices. An analysis for a universal all-pass ring resonator where loss exists in the coupling region has been presented by Han [33]. The analysis can be used as a guideline for the design of band-stop filters and other kinds of high performance plasmonic resonators which will find extensive applications.

A schematic of a universal ring resonator is shown in figure 2. When the coupling region has loss and non-zero physical length, the coupling coefficient κ and transmission coefficient τ are both complex numbers, and we assume

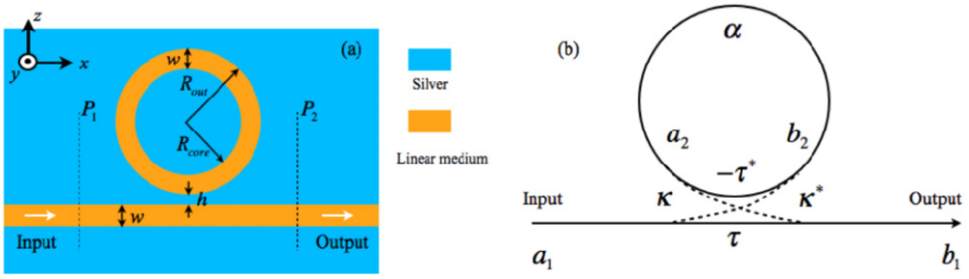

Figure 2. (a) Structure of a plasmonic filter structure where a circular ring resonator filled with linear material is coupled to a bus waveguide. (b) Schematic of a universal all-pass ring resonator with coupling loss [32].

$|\kappa|^2 + |\tau|^2 = \beta$ [33]. Under the conditions that a single unidirectional mode of the resonator is excited, the interaction can be described by the matrix relation [32]:

$$\begin{vmatrix} b_1 \\ b_2 \end{vmatrix} = \begin{vmatrix} \tau & \kappa \\ -\kappa^* & \tau^* \end{vmatrix} \begin{vmatrix} a_1 \\ a_2 \end{vmatrix} \tag{5}$$

and the transmission around the resonator is given by [32]:

$$a_2 = \alpha e^{i\theta} b_2 \tag{6}$$

where the real number α is the inner circulation factor describing the internal loss, with $\alpha = 1$ when there is no internal loss, and θ is the round-trip phase. From equations (3) and (4), we can get [33]:

$$b_1 = \frac{-\alpha\beta + \tau e^{-i\theta}}{-\alpha\tau^* + e^{-i\theta}} a_1, \qquad a_2 = \frac{-\alpha\kappa^*}{-\alpha\tau^* + e^{-i\theta}} a_1. \tag{7}$$

So the transmission passed by the resonator in the MIM bus waveguide is:

$$T = \frac{|b_1|^2}{|a_1|^2} = \frac{\alpha^2\beta^2 + |\tau|^2 - 2\alpha\beta|\tau|\cos(\theta + \phi_\tau)}{1 + \alpha^2|\tau|^2 - 2\alpha|\tau|\cos(\theta + \phi_\tau)} \tag{8}$$

where $\tau = |\tau|e^{i\phi_\tau}$. Under the resonance condition ($\theta + \phi_\tau = 2m\pi$, m is an integer), the transmission is:

$$T = \frac{(\alpha\beta - |\tau|)^2}{(1 - \alpha|\tau|)^2}. \tag{9}$$

Equations (7), (8) and (9) were deduced to investigate the transmission relation in a racetrack MIM resonator in [33]. Compared to dielectric ring resonators, MIM waveguides suffer from more loss in the ring and there is also some loss in the coupling region, so that α and β are relatively smaller than in the dielectric structures. Furthermore, τ is larger in the plasmonic device because more power goes through the straight bus waveguide due to the weak coupling [33]. By solving the dispersion equation of a MIM waveguide, the relation between α in the racetrack resonator and coupling region length can be obtained. τ, β and κ can be calculated separately in the coupling region by the FDTD method.

This kind of MIM ring resonator can be used as an all-optical filter and the filtering performance of the structure can be explained as follows. When the incident SPP wave passes through the bus waveguide it is partly coupled to the mode in the ring cavity which will begin to resonant in the cavity. After being partly decoupled into the bus waveguide in each resonant cycle, it interferes with the modes in the bus waveguide [11, 32, 33]. The resonant wavelength is determined by the resonance condition of the cavity $2\pi R_{\text{eff}} N_{\text{eff}} = m\lambda$, where R_{eff} is the effective radius and N_{eff} is the effective refractive index in the cavity which increases with the increase of the dielectric index in the cavity [11, 20, 21]. For simplicity, we assume the effective index of the bent MIM waveguide is the same as that of the straight MIM which is related to the refractive index and width of the MIM waveguide. Their dispersion relation can be expressed as [24, 34]

$$\tanh\left(\frac{w}{2}\sqrt{\beta_{\text{spp}}^2 - \varepsilon_{\text{d}} k_0^2}\right) = \frac{-\varepsilon_{\text{d}}\sqrt{\beta_{\text{spp}}^2 - \varepsilon_{\text{m}} k_0^2}}{\varepsilon_{\text{m}}\sqrt{\beta_{\text{spp}}^2 - \varepsilon_{\text{d}} k_0^2}} \tag{10}$$

where k_{m} and k_{d} are transverse propagation constants of the metal and dielectric and w is the width of the waveguide. ε_{m} and ε_{d} are the dielectric constants of the metal and cavity, respectively. β_{spp} stands for the complex propagation constant of the SPP waves. $k_0 = 2\pi/\lambda$ is the wavevector of the incident light. The effective index n_{eff} of the MIM waveguide as a function of wavelength can be solved from $n_{\text{eff}} = \beta_{\text{spp}}/k_0$.

Figure 3(a) shows the transmission spectra of the coupled ring cavity with different dielectric refractive indices when $w = 50$ nm, $h = 10$ nm and $R_{\text{core}} = 100$ nm. One can see that the central wavelength has a red-shift when the refractive index increases. In figure 3(b), we plot transmission valleys of two different resonant modes as a function of the refractive index of the material in the MIM waveguide. It is found that the stopped-wavelength grows steadily with increasing dielectric constant of the cavity in a wide spectral range. This relation implies a way to modulate the resonance by changing the dielectric constant, which can be implemented by embedding a nonlinear material into the ring resonator. Therefore, one can realize the narrow band filtering function at desired wavelengths by properly choosing the parameters of the coupled ring cavity and incident light.

4. Plasmonic filter with a circular ring resonator containing a nonlinear medium

It has been shown that when the dielectric material in the plasmonic waveguide exhibits a nonlinear response at optical frequencies, the power flow can be conveniently

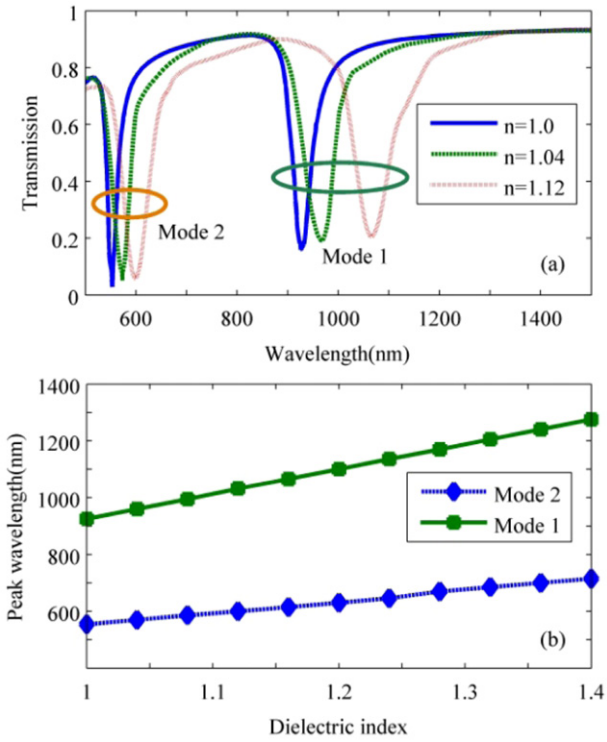

Figure 3. (a) Transmission spectra with different refractive indices with $w = 50$ nm, $h = 10$ nm and $R_{core} = 100$ nm. (b) The wavelengths of the transmission valleys as a function of the refractive index of the material in the MIM waveguide.

controlled with nonlinear effects [35, 36]. Any attempt to employ advanced features offered by a nonlinear plasmonic waveguide at high optical powers should begin by determining what effect nonlinearity in the dielectric layer would have on the dispersion of SPPs [37]. The exact dispersion relation for SPP modes of a plasmonic slot waveguide, which is formed by a nonlinear Kerr medium sandwiched between two metallic slabs, was presented in [37]. In our structure, the electric field distribution is quite uniform for most parts in the MIM gap region, except for the position very close to the edge of the metal layer. Without losing generality, the field in the waveguide can be considered as a uniform field. After a nonlinear material is introduced into the MIM waveguide, the variation in the dielectric constant induced by the nonlinear effect is also location dependent. Taking the width of the MIM waveguide as 50 nm and $\beta w < 2.5$, the approximate dispersion relation obtained using equation (8) agrees well with the exact relationship [37]. Consequently, the refractive index change in the gap region is also considered to be uniform. For larger β, the true dispersion branch bends downwards, the location-dependent field distribution and dielectric constant variation have been considered.

Figure 4 shows the transmission spectra plotted in a logarithmic form at different intensities of the incident light and the parameters of the structure are the same as that in figure 3 except for the material in the MIM waveguide. In this case, a circular ring resonator filled with nonlinear material is coupled to the bus waveguide that was shown in figure 1. The intensity is determined by $|E|^2$ which represents the square

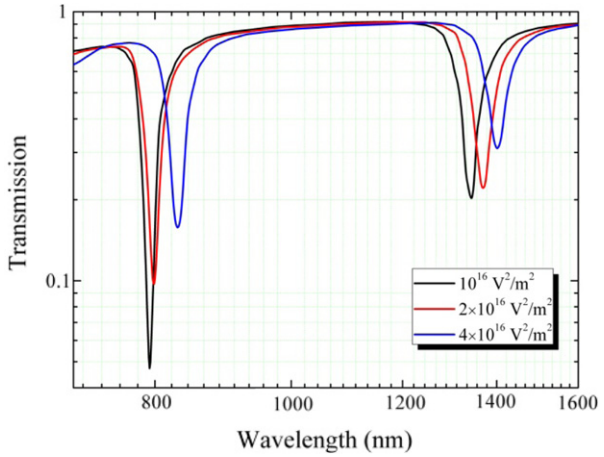

Figure 4. Transmission spectra of the structure plotted in a logarithmic form shown in figure 1 at incident intensities of 10^{16}, 2×10^{16} and 4×10^{16} V^2 m^{-2}. The dielectric constant of the nonlinear material is determined by equation (2). The other parameters of the structure are the same as in figure 3.

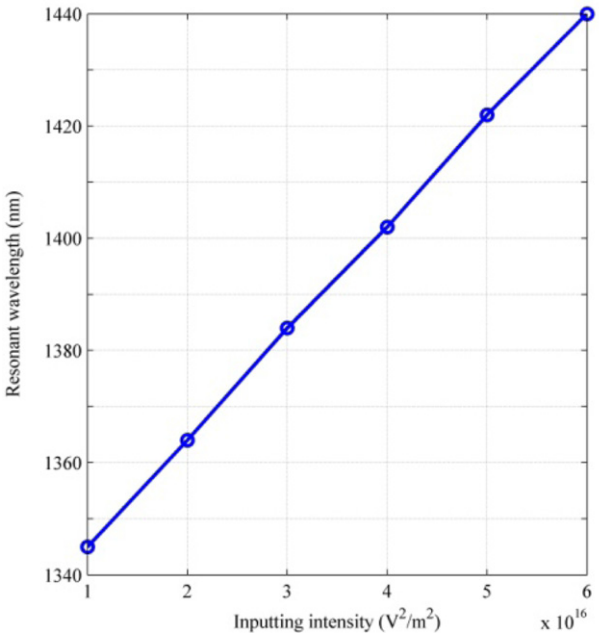

Figure 5. Resonant wavelength for the first mode of the designed band-stop filter as a function of optical input intensity.

of amplitude (peak value) of the incident light and $|E|^2$ are chosen as 10^{16}, 2×10^{16} and 4×10^{16} V^2 m^{-2}. We can see that the transmitted-valley has a red-shift with the increase in the intensity of the incident light. This phenomenon is due to the increase in the incident intensity which will augment the refractive index of the Kerr medium, and results in the red-shift of the resonance wavelength according to the result in figure 3(b). This structure possesses an obvious wavelength-filtering function.

Figure 5 shows the resonant wavelength for the first mode of the designed band-stop filter for different input intensities; all the other parameters are the same as in figure 4. One can

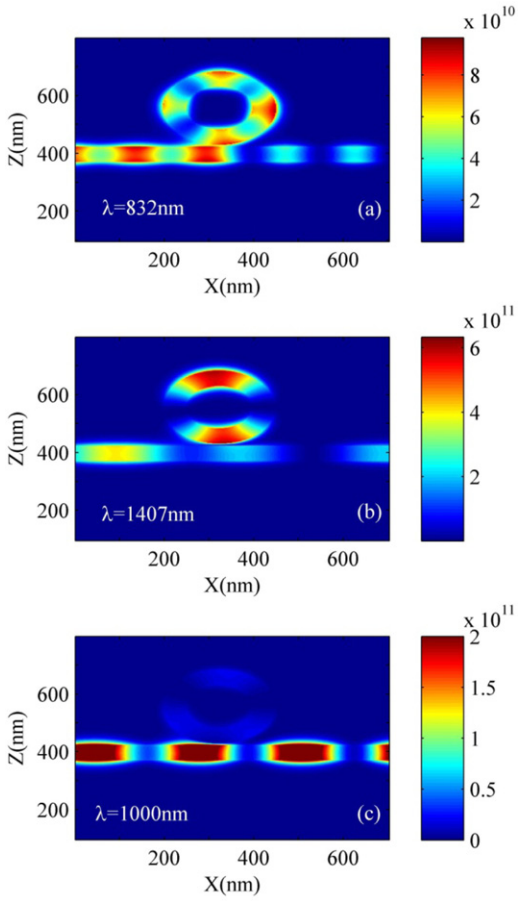

Figure 6. (a) The $|H_y|$ field pattern of simple band-stop filter at the second resonance wavelength of 832 nm. (b) The $|H_y|$ field profile of the filter at the first resonance wavelength of 1407 nm. (c) The $|H_y|$ field profile of the filter at non-resonance wavelength of 1000 nm.The incident intensity is 4×10^{16} V^2 m^{-2}.

find that in this case, the resonant wavelength increase nearly linearly with input intensity.

Figures 6(a)–(c) depict the contour profiles of the field $|H_y|$ for different wavelengths when the incident intensity is 4×10^{16} V^2 m^{-2}. The field distributions in figures 6(a) and (b) correspond to the second and first resonances in figure 4, respectively. One can see that when the standing waves form in the ring at resonance, only a small number of SPPs can propagate through the filter for the two resonant wavelengths. Modes 1 (1407 nm) and 2 (832 nm) form standing waves in the ring with one and two antinodes/nodes respectively as seen in figures 6(b) and (a). For a frequency of the incident wave far from the resonance frequency, the cavity mode is not excited and therefore transmits through the bus waveguide that can be seen in figure 6(c) as an example. As the wavelength of the second mode is shorter than that of the first one, so the power density of the second resonance is higher than the first one. Therefore, more power can be coupled into the ring at the coupling region for the second mode, so the second resonance mode has a stronger coupling to the ring in comparison with the first one [22].

To further verify the transmission response at different input intensities, the contour profiles of field $|H_y|$ at the

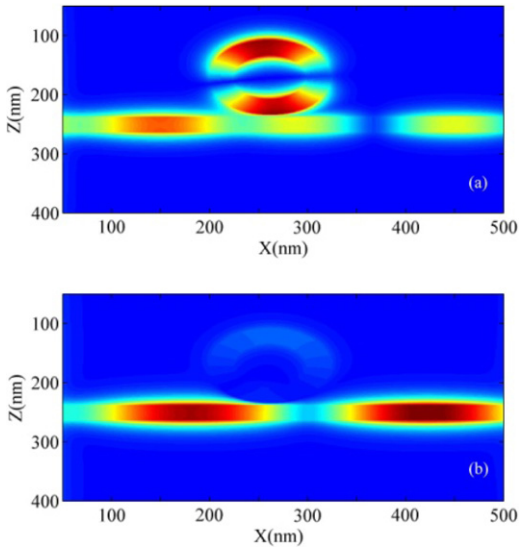

Figure 7. Contour profiles of field $|H_y|$ at the incident electric intensity of (a) 10^{16} V^2 m^{-2} and (b) 4×10^{16} V^2 m^{-2} at the wavelength of 1350 nm.

intensities of 10^{16} V^2 m^{-2} and 4×10^{16} V^2 m^{-2} at the wavelength of 1350 nm are plotted in figures 7(a) and (b), respectively. It is obvious that when the incident intensity is 10^{16} V^2 m^{-2} the transmission for the wavelength is low, and by increasing the intensity to 4×10^{16} V^2 m^{-2} the same wavelength now is transmitted by the structure.

Even though higher field confinement implies higher propagation losses, MIM structures have been successfully employed in resonant structures for wavelength-filtering applications [11, 13, 17]. A key aspect of any wavelength filter device is to be able to provide high wavelength selectivity, which means a high quality factor Q. The quality factor of this filtering system can be defined as $Q = \lambda_{res}/\Delta\lambda$, where λ_{res} is the resonant wavelength of the ring cavity and $\Delta\lambda$ is the full width at half maximum of the transmission spectra. When the intensity of the incident light is 10^{16} V^2 m^{-2}, the quality factors of the first mode and the second mode are, respectively, 25.86 and 39.65. There is some deterioration of the filtering characteristics for increasing intensities, which can be seen from figure 4. By increasing the intensity to 4×10^{16} V^2 m^{-2}, the quality factors of the first mode and the second mode decrease to 18.22 and 25.18, respectively.

Our structure can be operated as a plasmonic band-stop filter, which is different from the band-pass filters in [19–21]. The proposed filter structure has a very simple structure and the transmission spectrum of this system possesses obvious and sharp valleys. In conjunction with a nonlinear medium, the resonance wavelength of the cavity can be tuned by changing the incident intensity, without changing the outer size of the structure. Besides, the modulation of transmission (resonant) valleys can be realized in a broad wavelength range which may have promising applications in nano-photonics.

5. Conclusions

In this paper, we have presented a novel nano-scale all-optical filter consisting a MIM waveguide coupled to circular ring

resonator containing a nonlinear medium. The propagation characteristics have been studied by the FDTD method. The simulation results show that the stopped-wavelength can be tuned by changing the intensity of the incident light. By increasing the intensity of the incident light, the resonant wavelengths of the structures experience a red-shift. Our structure can decrease plasmonic filter dimensions so will find potential applications in all-optical communication in highly integrated optical circuits and optical computing.

Acknowledgments

Project supported by the National Natural Science Foundation of China (grant no 20907021) and the Foundation for Outstanding Young Teachers of Nanjing University of Information Science & Technology. The authors would especially like to thank Dr Xu Yi from South China Normal University for his useful discussions and the use of Rsoft's FullWAVE software package.

References

[1] Barnes W L, Dereux A and Ebbesen T W 2003 Surface plasmon subwavelength optics *Nature* **424** 824
[2] Ozbay E 2005 Plasmonics: merging photonics and electronics metal slit structures *Opt. Express* **13** 9652
[3] Bozhevolnyi S I, Volkov V S, Devaux E and Ebbesen T W 2005 Channel plasmon-polariton guiding by subwavelength metal grooves *Phys. Rev. Lett.* **95** 046802
[4] Bozhevolnyi S I, Volkov V S, Devaux E, Laluet J Y and Ebbesen T W 2006 Channel plasmon subwavelength waveguide components including interferometers and ring resonators *Nature* **440** 508
[5] Berini P 2008 Bulk and surface sensitivities of surface plasmon waveguides *New J. Phys.* **10** 105010
[6] Donghyun K 2005 Effect of the azimuthal orientation on the performance of grating-coupled surface-plasmon resonance bio-sensors *Appl. Opt.* **44** 3218
[7] Hosseini A and Massoud Y 2006 A low-loss metal–insulator–metal plasmonic bragg reflector *Opt. Express* **14** 11318
[8] Wang B and Wang G P 2005 Plasmon Bragg reflectors and nanocavities on flat metallic surfaces *Appl. Phys. Lett.* **87** 013107
[9] Han Z, Forsberg E and He S L 2007 Surface plasmon Bragg gratings formed in metal–insulator–metal waveguides *IEEE Photon. Technol. Lett.* **19** 91
[10] Qiao M, Claus B, Marthandam P and Gordon R 2008 Plasmonic bragg reflectors: optimization and application to isolation *IEEE J. Sel. Top. Quantum Electron.* **14** 1502
[11] Wang T B, Wen X W, Yin C P and Wang H Z 2009 The transmission characteristics of surface plasmon polaritons in ring resonator *Opt. Express* **17** 24096
[12] Gan Q Q, Ding Y J and Bartoli F J 2009 'Rainbow' trapping and releasing at telecommunication wavelengths *Phys. Rev. Lett.* **102** 056801
[13] Lin X S and Huang X G 2008 Tooth-shaped plasmonic waveguide filters with nanometeric sizes *Opt. Lett.* **33** 2874
[14] Li X F, Pan S, Guo Y N and Wang Q 2011 Control of plasmonic wave propagating in nanocavity with tooth-shaped configuration *Chin. Phys.* B **20** 015204
[15] Matsuzaki Y, Okamoto T, Haraguchi M, Fukui M and Nakagaki M 2008 Characteristics of gap plasmon waveguide with stub structures *Opt. Express* **16** 16314
[16] Noual A, Akjouj A, Pennec Y, Gillet J-N and Djafari-Rouhani B 2009 Modeling of two-dimensional nanoscale Y-bent plasmonic waveguides with cavities for demultiplexing of the telecommunication wavelengths *New J. Phys.* **11** 103020
[17] Xiao S S, Liu L and Qiu M 2006 Resonator channel drop filters in a plasmon–polaritons metal *Opt. Express* **14** 2932
[18] Hosseini A and Massoud Y 2007 Nanoscale surface plasmon based resonator using rectangular geometry *Appl. Phys. Lett.* **90** 181102
[19] Yun B F, Hu G H and Cui Y P 2010 Theoretical analysis of a nanoscale plasmonic filter based on a rectangular metal–insulator–metal waveguide *J. Phys. D: Appl. Phys.* **43** 385102
[20] Lu H, Liu X M, Gong Y K, Wang L R and Dong M 2011 Multi-channel plasmonic waveguide filters with disk-shaped nanocavities *Opt. Commun.* **284** 2613
[21] Setayesh A, Mirnaziry S R and Abrishamian M S 2011 Numerical investigation of a tunable band-pass plasmonic filter with a hollow-core ring resonator *J. Opt.* **13** 035004
[22] Wurtz G A, Pollard R and Zayats A V 2006 Optical bistability in nonlinear surface-plasmon polaritonic crystals *Phys. Rev. Lett.* **97** 057402
[23] Porto J A, Moreno L M and Garcia-Vidal F J 2004 Optical bistability in subwavelength slit apertures containing nonlinear media *Phys. Rev.* B **70** 081402
[24] Min C J, Wang P, Jiao X J, Deng Y and Ming H 2007 Beam manipulating by metallic nano-optic lens containing nonlinear media *Opt. Express* **15** 9541
[25] Min C J, Wang P, Chen C C, Deng Y, Lu Y H, Ming H, Ning T Y, Zhou Y L and Yang G Z 2008 All-optical switching in subwavelength metallic grating structure containing nonlinear optical materials *Opt. Lett.* **33** 869
[26] Wang G X, Lu H, Liu X M, Gong Y K and Wang L R 2011 Optical bistability in metal–insulator–metal plasmonic waveguide with nanodisk resonator containing Kerr nonlinear medium *Appl. Opt.* **50** 5287
[27] Lin X S, Yan J H, Zheng Y B, Wu L Y and Lan S 2011 Dependencey of resonant wavelength on the width of subwavelength metallic slits: analysis and modulation *J. Phys.: Conf. Ser.* **276** 012070
[28] Zhong Z J, Xu Y, Lan S, Dai Q F and Wu L J 2010 Sharp and asymmetric transmission response in metal–dielectric–metal plasmonic waveguides containing Kerr nonlinear media *Opt. Express* **18** 79
[29] Rakic A D, Djurisic A B, Elazar J M and Majewski M L 1998 Optical properties of metallic films for vertical cavity optoelectronic devices *Appl. Opt.* **37** 5271
[30] Fujii M, Koos C, Poulton C, Sakagami I, Leuthold J and Freude W 2005 A simple and rigorous verification technique for nonlinear FDTD algorithms by optical parametric four-wave mixing *Microw. Opt. Technol. Lett.* **48** 88
[31] Johnson P B and Christy R W 1972 Optical constants of the noble metals *Phys. Rev.* B **6** 4370
[32] Yariv A 2000 Universal relations for coupling of optical power between microresonators and dielectric waveguides *Electron. Lett.* **36** 321
[33] Han Z 2010 Ultracompact plasmonic racetrack resonators in metal–insulator–metal waveguides *Photon. Nanostruct.* **8** 172
[34] Gordon R and Brolo A 2005 Increased cut-off wavelength for a subwavelength hole in a real metal *Opt. Express* **13** 1933
[35] Davoyan A R, Shadrivov I V, Zharov A A, Gramotnev D K and Kivshar Y S 2010 Nonlinear nanofocusing in tapered plasmonic waveguides *Phys. Rev. Lett.* **105** 116804
[36] Feigenbaum E and Orenstein M 2007 Plasmon soliton *Opt. Lett.* **32** 674
[37] Rukhlenko I D, Pannipitiya A and Premaratne M 2011 Dispersion relation for surface plasmon polaritons in metal/nonlinear–dielectric/metal slot waveguides *Opt. Lett.* **33** 3374